JGP Journal of General Physiology

METHODS AND APPROACHES

Wheat germ agglutinin–conjugated fluorescent pH sensors for visualizing proton fluxes

Lejie Zhang[1], Mei Zhang[1], Karl Bellve[3], Kevin E. Fogarty[3], Maite A. Castro[4,6,8], Sebastian Brauchi[5,6,7,8], and William R. Kobertz[1,2]

Small-molecule fluorescent wheat germ agglutinin (WGA) conjugates are routinely used to demarcate mammalian plasma membranes, because they bind to the cell's glycocalyx. Here, we describe the derivatization of WGA with a pH-sensitive rhodamine fluorophore (pHRho; pKa = 7) to detect proton channel fluxes and extracellular proton accumulation and depletion from primary cells. We found that WGA-pHRho labeling was uniform and did not appreciably alter the voltage gating of glycosylated ion channels, and the extracellular changes in pH correlated with proton channel activity. Using single-plane illumination techniques, WGA-pHRho was used to detect spatiotemporal differences in proton accumulation and depletion over the extracellular surface of cardiomyocytes, astrocytes, and neurons. Because WGA can be derivatized with any small-molecule fluorescent ion sensor, WGA conjugates should prove useful to visualize most electrogenic and nonelectrogenic events on the extracellular side of the plasma membrane.

Introduction

Approaches that specifically target fluorescent biosensors to cellular domains are of great interest, because they are valuable tools to investigate physiological activity in cells, tissues, and living organisms. Indeed, a review of biosensors that primarily targeted intracellular compartments was published in the *Journal of General Physiology* in 2017 (Pendin et al., 2017). In contrast, there is a paucity of approaches that target fluorescent biosensors to detect ions and metabolites on the extracellular side of the plasma membrane (Marvin et al., 2013; Patriarchi et al., 2018; Lobas et al., 2019; Sun et al., 2018). A substantial stumbling block is optimizing the protein biosensor to properly fold in the ER and traffic uniformly to the plasma membrane. To avoid the secretory pathway, we previously described a bioorthogonal chemistry approach that targets small-molecule fluorescent pH sensors to the cell's glycocalyx for the real-time visualization of extracellular proton accumulation and depletion (Zhang et al., 2016). Although our first approach detected proton fluxes at the plasma membrane from ion channels and membrane transport proteins, it required cells to use and efficiently incorporate an unnatural sialic acid precursor into the glycocalyx. In addition, the calculated changes in pH were approximations, because we had to assume the cell surface labeling was constant over the entire plasma membrane. Therefore, we sought a simplified approach that would work with most cells and provide calibrated changes in extracellular pH adjacent to the plasma membrane.

Small-molecule wheat germ agglutinin (WGA) conjugates appear to be well suited to target biosensors to the glycocalyx, because fluorescent WGA conjugates are commonly used to demarcate the plasma membrane of fixed cells. Although prone to photobleaching and internalization, WGA-fluorescein has been used to approximate extracellular pH at the glycocalyx (Villafuerte et al., 2014; Stock et al., 2007; Schroeder et al., 2013), raising the possibility that pH-sensitive WGA conjugates may enable the visualization of extracellular proton fluxes from voltage-gated ion channels, membrane transport proteins, and proton omega currents that have been associated with human disease (Fig. 1).

Here, we describe the synthesis and utilization of WGA with a pH-sensitive rhodamine fluorophore (pHRho; Fig. 1 A), a red

[1]Department of Biochemistry and Molecular Pharmacology, University of Massachusetts Medical School, Worcester, MA; [2]Programs in Neuroscience and Chemical Biology, University of Massachusetts Medical School, Worcester, MA; [3]Biomedical Imaging Group, Molecular Medicine, University of Massachusetts Medical School, Worcester, MA; [4]Department of Biochemistry and Microbiology, Universidad Austral de Chile, Campus Isla Teja, Los Rios, Chile; [5]Department of Physiology, Universidad Austral de Chile, Campus Isla Teja, Los Rios, Chile; [6]Center for the Interdisciplinary Studies on Nervous System, Universidad Austral de Chile, Campus Isla Teja, Los Rios, Chile; [7]Millennium Nucleus of Ion Channel-Associated Diseases (MiNiCAD), Valdivia, Chile; [8]Janelia Research Campus, Howard Hughes Medical Institute, Ashburn, VA.

Correspondence to William R. Kobertz: william.kobertz@umassmed.edu

This work is part of the special collection entitled "Electrical Signaling in the Heart and Nervous System: A Joint Meeting of the Society of General Physiologists and Latin American Society of Biophysicists."

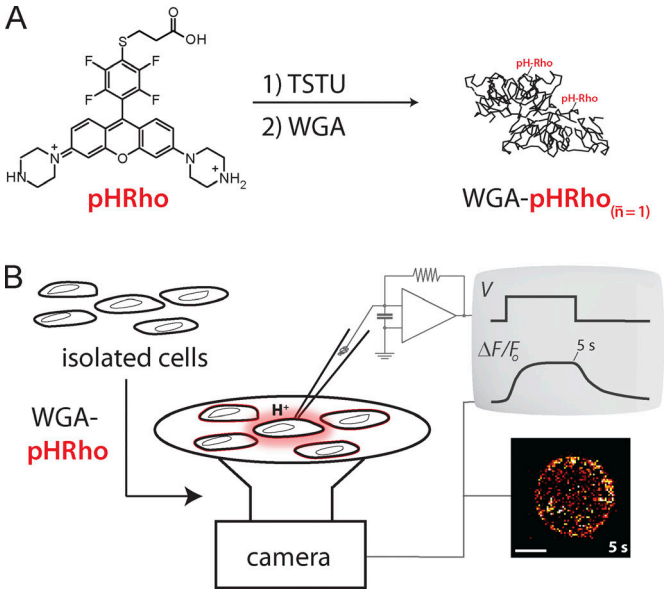

Figure 1. **Derivatization of WGA with a small-molecule fluorescent pH sensor and cell surface labeling to visualize plasma membrane proton fluxes. (A)** Synthetic scheme of WGA-pHRho. Using the degree of labeling equation (Materials and methods) on average, one WGA monomer is labeled with one pHRho molecule that is activated with N,N,N′,N′-tetramethyl-O-(N-succinimidyl) uronium tetrafluoroborate (TSTU). The doubly labeled WGA homodimer is shown. **(B)** Cartoon depiction of the whole-cell patch-clamp fluorometry approach to visualize proton fluxes with WGA-pHRho.

fluorescent WGA conjugate to visualize extracellular proton accumulation and depletion. Although WGA binds to the terminal sugars of glycosylated proteins, labeling cells with WGA conjugates did not appreciably alter the voltage gating of glycosylated or nonglycosylated ion channels. Extracellular proton fluxes were fluorescently detected from cells coated with either WGA-pHRho or WGA-fluorescein 4 h after labeling, despite visual signs of endocytosis. Compared with WGA-fluorescein, WGA-pHRho was photostable, increased fluorescence upon protonation, and has a pKa of ∼7 (Aigner et al., 2012) that is well matched for extracellular pH determinations. On-cell calibration of WGA-pHRho and WGA-fluorescein provided accurate changes of pH over the extracellular surface of mammalian cells. Using various imaging modalities, differential extracellular proton accumulation and depletion was detected (1) at the sarcolemma and tranverse tubules (t-tubules) of cardiomyocytes and (2) in neuron–astrocyte cocultures. This straightforward approach and the detailed procedures for WGA conjugation and cell surface labeling will enable physiologists and biophysicists to employ these reagents to fluorescently visualize proton fluxes and to spatiotemporally determine extracellular pH changes adjacent to the plasma membrane.

Materials and methods

WGA-pHRho synthesis

pHRho was synthesized by deprotection of compound 3 in Zhang et al. (2016) with 4 M HCl. After stirring for 4 h, the solvent was evaporated under reduced pressure, and pHRho was purified by HPLC using a C18 column (4.6 mm × 250 mm) eluting with solvent A (0.1% trifluoroacetic acid) and solvent B (acetonitrile); gradient 5–95% B over 30-min pHRho (1.0 mg, 1.4 µmol) was reacted with 14 µmol N,N,N′,N′-tetramethyl-O-(N-succinimidyl) uronium tetrafluoroborate in 200 µl anhydrous N,N-dimethylformamide at room temperature for 1 h. The above reaction mixture (100 µl) was added to 1 mg WGA (Vector Laboratories) for a 5:1 dye/WGA molar ratio in 1 ml of 0.1 M sodium bicarbonate (pH 8.3) containing 120 mg N-acetylglucosamine. The reaction mixture was stirred at room temperature for 2 h and was terminated by adding 6.25 µl of a hydroxylamine solution to a final concentration of 0.1 M. Commercially available WGA-fluorescein was purchased from Vector Laboratories. For homemade WGA-fluorescein, a FITC stock solution was prepared at 10 mg/ml in N,N-dimethylformamide immediately before starting the reaction, and 0.26 µmol FITC dye was added to WGA solution with N-acetylglucosamine (pH 9.0); the final dye/WGA ratio was 10:1. The WGA conjugates were separated from unreacted fluorophore by gravity gel filtration on a Sephadex G-25 Fine (20–50 µm) column equilibrated in PBS, and final samples were lyophilized down to a powder. The degree of labeling (DOL) was calculated using the following equation, and the absorbance of WGA conjugate was measured at 280 nm (A_{280}) and the λ_{max} (A_{max}):

$$DOL = \frac{A_{max} \times MW}{[WGA] \times \varepsilon_{dye}},$$

where MW is the molecular weight of WGA, ε_{dye} is the extinction coefficient of the dye at its absorbance maximum, and the WGA protein concentration is in milligrams per milliliter (fluorescein: ε_{494} = 68,000 $M^{-1}cm^{-1}$; pHRho: ε_{590} = 120,000 $M^{-1}cm^{-1}$).

Chinese hamster ovary (CHO) cell labeling with pH-sensitive WGA conjugates, cell surface calibration, and whole-cell patch-clamp fluorometry

CHO cell culture and transfection procedures were conducted as previously described (Zhang et al., 2016); a plasmid containing cytoplasmic eGFP or mCherry (0.25 µg) was added to the transfection mixtures to identify transiently transfected cells. Transfected CHO cells were trypsinized and seeded on a glass-bottom culture dish for 2 h, labeled with WGA conjugates (50 µg/ml) in Hanks' buffered saline solution (HBSS) at room temperature for 10 min, and then rinsed with bath solution (in mM): 145 NaCl, 5.4 KCl, 2 $CaCl_2$, and 0.1 buffer (HEPES for pH 7.5 and Mes for pH 6.0) with NaOH. Table 1 lists the cell-type labeling conditions with WGA-pHRho. Whole-cell voltage-clamp fluorometry was performed (Zhang et al., 2016) using internal solution (in mM): 126 KCl, 2 $MgSO_4$, 0.5 $CaCl_2$, 5 EGTA, 4 K_2-ATP, 0.4 guanosine triphosphate, and 25 buffer (HEPES for pH 7.5 and Mes for pH 6.0). Cells were imaged at 10 Hz using a CoolLED pE-4000 light source (exposure time, 10 ms), 63 × 1.4 numerical aperture oil-immersion objective, and a Zyla sCMOS camera (Andor). WGA-fluorescein and WGA-pHRho were excited respectively at 490- and 550-nm channels (Chroma 89402 emission filter set). Fluorescent images were collected (4 × 4 binning) and processed using ImageJ software.

Table 1. **WGA-pHRho labeling of various cells**

Conditions	Cell lines	Cardiomyocytes	Neuron–astrocyte cocultures
$[WGA\text{-}pHRho]_{final}$ (mg/ml)	50	50	100
Buffer	HBSS	HBSS	GBFM
Time (min)	10	30	20
Temperature	RT	RT	RT

Rat ventricular myocyte isolation, WGA-pHRho labeling, and structured light microscopy

Rat ventricular myocytes were isolated from adult Sprague-Dawley rats (200–250 g) by enzymatic (Liberase; Roche) digestion (Colecraft et al., 2002). Animals were anaesthetized with ketamine/xylazine (100 mg/kg:10 mg/kg) under the guidelines of the University of Massachusetts Medical School Animal Care and Use Committee. Hearts were excised and ventricular myocytes were isolated using Langedorff perfusion. Healthy, rod-shaped cardiomyocytes were cultured in Medium 199 on laminin-coated glass-bottom culture dishes with 5% CO_2 and 95% air at 37°C for 2 h before imaging experiments. Cardiomyocytes were incubated with WGA-pHRho (50 µg/ml) in HBSS buffer at room temperature for 30 min. Cells were first perfused with Tyrode's solution (in mM): 145 NaCl, 5.4 KCl, 2 $CaCl_2$, 1 $MgCl_2$, and 0.1 HEPES (pH 7.5) and then with 10 mM lactate in Tyrode's solution. The monocarboxylate transporter 1 (MCT-1) inhibitor AR-C155858 (50 nM) was added to the cardiomyocytes for 30 min at room temperature before lactate perfusion. Cardiomyocytes were imaged on TESM, a custom-built microscope system that has TIRF and structured illumination wide-field epifluorescence for fast optical sectioning and enhanced spatial resolution (Navaroli et al., 2012). The structured light images were formed by illuminating through a grating (500 lines-pairs/in) on a Physik Instruments translation stage that was moved one third and two thirds of a period (~2 ms) for the second and third images. The three structured light images (180 sets of 3 × 50-ms exposures at 1 Hz) were collected at a focal plane 1.8 µm above the coverslip on an inverted Olympus IX71 microscope with a 60 × 1.49 numerical aperture oil-immersion objective with a 1.6× optivar. The sample was illuminated with a Cobolt diode-pumped solid-state 100-mW laser (561 nm) and the emission collected onto a 1,004 × 1,002 Andor iXon 885 emCCD camera, which was binned at 2 × 2.

Structured illumination image processing and concentric annuli analysis

All image processing was performed using custom software, but the operations are available in ImageJ. At each time point, the three unprocessed structure illumination grating position images were added (corresponding x, y pixels) to reject out-of-focus light (Neil et al., 1997) and produce a wide-field equivalent image with higher signal-to-noise. The processed images were corrected for any remaining locally diffuse fluorescence background by subtracting the morphological opening (maximum of the minimums) of each time point using a radius of 10 pixels (1.67 µm), which removes the local background while preserving bright objects smaller than ~3 µm. To generate a closed (2-D) outline of the cell, a maximum intensity projection was made from the first 30 preperfusion frames of the time series and the outermost visible boundary of the sarcolemma manually traced. The concentric binary (0|1) annular masks were generated by creating a mask of the entire cell and applying a morphological binary erosion of 5 pixels (835 nm) and then subtracting this smaller mask from the original to create annular mask A0. Annular masks A1–A3 were generated by repeating the process using the smaller mask as the starting point. Using these 2-D annular masks, the total and average (normalized for area) fluorescence signal of each annulus was calculated at each time point of the processed image series. The fluorescent signal from the whole cell was calculated using the cell outline mask. The computed average signal over time, F(t) for the whole cell and each annulus, was converted to percent change in signal, $\Delta F/F_0 = 100 \times [F(t) - F_0]/F_0$, using the average of the preperfusion time points as F_0.

WGA-pHRho labeling and imaging of primary astrocyte and neuron cocultures

Astrocyte and neuron cocultures were obtained from postnatal day 1 pups of C57bl/6 mice. All C57bl/6 (females and males, 1 d old) were obtained from the Biosecurity Laboratory Facility for Animal Experimentation (Janelia Research Campus, Howard Hughes Medical Institute). All procedures were conducted in accordance with protocols approved by the Janelia Institutional Animal Care and Use Committee. Forebrains were removed and the cortex dissected. Tissue was digested with 0.12% trypsin (wt/vol; Gibco) in 0.1 M phosphate buffer (PBS, pH 7.4, osmolarity 320 mOsm) and mechanically disrupted with a fire-polished Pasteur pipette. Cells were plated at 0.3 × 10^6 cells/cm^2 in glass-bottom dishes (Cellvis) coated with poly-L-lysine (mol wt >350 kD; Sigma-Aldrich), and cultured for up to 10 d in Nbactive4 (BrainBits) medium supplemented with 3% fetal bovine serum. Cultured cells were incubated for 30 min in 500 µl of glucose- and buffer-free medium (GBFM) containing (in mM): 140 NaCl, 20 KCl, 2 $CaCl_2$, and 2 $MgCl_2$. During the last 20 min of glucose deprivation, 50 µl of WGA-pHRho (1 mg/ml) was added to the incubation media. The cells were rinsed three times with GBFM and imaged. Imaging was performed at 37°C, 5% CO_2 chamber on an inverted Zeiss LSM 880 microscope with a 63 × 1.4 numerical aperture oil-immersion objective equipped with an Airyscan array detector. The astrocyte and neuronal planes were imaged at 2 Hz (50-ms exposures) using 405- and 561-nm laser lines for DAPI and WGA-pHRho, respectively. Glucose (3 mM final concentration) and rotenone (100 µM final concentration) were directly added to the recording chamber on each running experiment. Changes in intensity values were

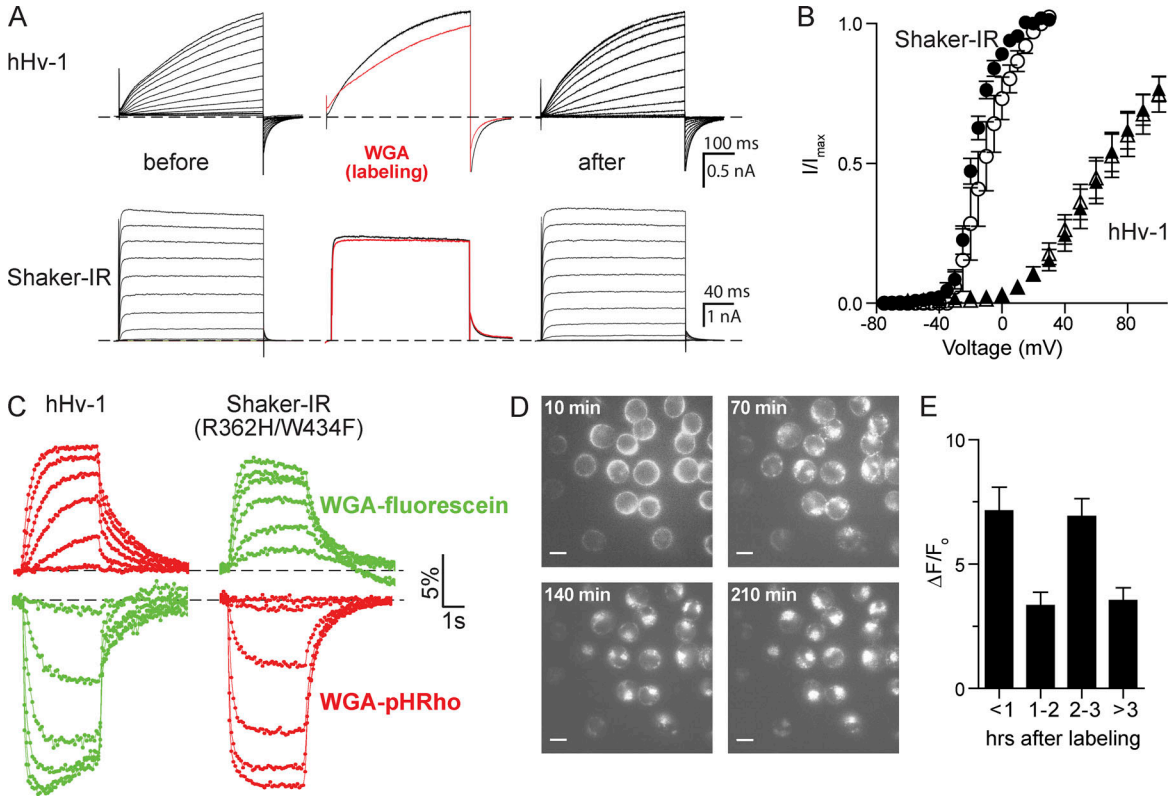

Figure 2. **WGA labeling and voltage-clamp fluorometry of CHO cells expressing voltage-gated channels. (A)** hHv-1 (top) and Shaker-IR (bottom) currents were recorded before (left) and after (right) WGA labeling (50 µg/ml). Middle panels are currents before (black) and after (red) WGA wash-in at 60 mV. Cells were held at −80 mV, hHv-1 depolarized for 0.5 s from −50 to 100 in 10-mV increments, and Shaker-IR depolarized for 0.2 s from −70 to 60 mV in 10-mV increments. **(B)** G-V curves of hHv-1 ($V_{0.5}$ = 68 ± 6 mV, *n* = 8, triangles) and Shaker-IR ($V_{0.5}$ = −18 ± 1 mV, *n* = 5, circles) before (closed) and after (open) WGA treatment. hHv-1: $V_{0.5}$ = 67 ± 8 mV, *n* = 9; Shaker-IR: $V_{0.5}$ = −11 ± 1 mV, *n* = 6. **(C)** Voltage-clamp fluorometry traces from cells labeled with WGA-pHRho (red) and homemade WGA-fluorescein (green). hHv-1 (left) was held at −80 mV, and changes in fluorescence were elicited from 4-s depolarizations from 0 to 100 mV in 20-mV increments. Shaker-IR R362H (right) was held at 30 mV, and fluorescence was elicited from 4-s command voltages from −120 to −20 mV in 20-mV increments. **(D)** Representative fluorescent images of CHO cells 10–210 min after labeling with WGA-pHRho for 30 min; scale bars represent 10 µm. **(E)** Bar graph of $\Delta F/F_0$ from hHv-1 expressing cells after a 4-s 80-mV depolarization versus time after WGA-pHRho labeling. *n* = 3 experiments. Error bars represent SEM.

calculated in ImageJ using maximum intensity projection series. Glucose and rotenone were obtained from Sigma-Aldrich. Acquisition, visualization, and Airyscan postprocessing were performed using Zen software (Zeiss), analysis was performed with ImageJ, and data plots were generated with Microcal Origin 9.

Online supplemental material

Fig. S1 is additional characterization of the WGA fluorescent pH sensor conjugates. Fig. S2 shows current–voltage relationships for hHv-1 and Shaker-IR (R362H/W434F) in an external low-buffer capacity solution and voltage-clamp fluorometry of CHO cells transfected with pCDNA3.1(−) and WT Shaker-IR plasmid DNA (negative controls for Fig. 2 C). Video 1 shows a $\Delta F/F_0$ movie of a representative CHO cell expressing Hv-1. Video 2 shows raw fluorescent images of a representative CHO cell expressing Shaker-IR (R362H/W434F) labeled with WGA-pHRho.

Results

We were initially concerned that WGA binding to the terminal sugars of a cell's glycocalyx would drastically alter voltage gating by either binding to glycosylated voltage sensors or shielding the negatively charged sialic acids that have been implicated in voltage gating (Johnson and Bennett, 2008; Johnson et al., 2004; Schwetz et al., 2011; Noma et al., 2009). To test the effects of WGA on voltage-gated ion channels, we recorded families of currents from cells transiently transfected with a voltage-gated proton (hHv-1) or potassium (Shaker-IR) channels before and after treatment with WGA (Fig. 2 A). hHv-1 cannot be N or O glycosylated (it does not contain any extracellular threonines or serines), whereas Shaker-IR contains two N-linked glycosylation sites in the S1-S2 loop of the voltage sensor. Tail current analysis showed that WGA treatment did not significantly affect the midpoint of voltage activation ($V_{1/2}$) of hHv-1 (Fig. 2 B). WGA perfusion (Fig. 2 A, middle) did slightly alter hHv-1 activation and deactivation kinetics; however, these subtle changes were due to WGA binding to endogenous glycoproteins, because hHv-1 does not have any extracellular serine or threonine residues and cannot be glycosylated. In contrast, Shaker-IR activation/deactivation gating was unaffected by WGA perfusion. WGA binding to N-glycosylated Shaker-IR channels did cause a small but statistically insignificant shift in $V_{1/2}$ (Fig. 2 B).

Given that unglycosylated and glycosylated voltage-gated ion channels were minimally affected by WGA treatment, we next determined whether pH-sensitive WGA conjugates would effectively report on proton accumulation and depletion on the extracellular side of the plasma membrane. The synthesis, activation, and conjugation of rhodamine-based pHRho to WGA (Fig. 1 A) is described in the Materials and methods. The WGA conjugation reaction was quenched with hydroxylamine and the quenched dye and excess N-acylgalactosamine (to protect the amino groups in the carbohydrate binding sites) were removed with a gravity-fed size-exclusion column (Materials and methods). Conjugation of the small-molecule pH-sensitive fluorophore to WGA did not significantly change the reported pKa (Aigner et al., 2012) or proton-dependent change in fluorescence (Fig. S1 A). Based on the protein-fluorophore absorbance ratio, on average, each WGA monomer was labeled with 1.0–1.1 pHRho molecules.

To fluorescently visualize proton efflux with WGA-pHRho, cells were treated with 50 µg/ml WGA-pHRho for 10 min, and the currents and fluorescence were measured using patch-clamp fluorometry in a bath solution with a low buffer capacity (0.1 mM). The top left panel in Fig. 2 C shows families of fluorescent signals from a CHO cell expressing hHv-1 that was labeled with WGA-pHRho. Under these low buffering conditions, voltage activation of hHv-1 channels resulted in small currents (Fig. S2 A) that reached steady state faster with stronger depolarizations. Simultaneous imaging of the cell's fluorescence at 10 Hz showed that the change in fluorescence was similar to the voltage dependence of hHv-1; however, the rate to reach steady state was slower, as it corresponded to proton accumulation at the cell surface and not hHv-1 channel gating (Figs. 2 C and S2 A). This distinction between channel gating and proton accumulation (or depletion) was evident upon hHv-1 deactivation at −80 mV; no current remained after 300 ms, whereas it required seconds for the fluorescent signal to fully decay. As we have had previously observed (Zhang et al., 2016), the fluorescent signal decay has two time constants; the fast component corresponds to protons rushing into the cell before hHv-1 channel closing, and the slow component corresponds to diffusion into bulk solution. A video of F/F_o snapshots before, during, and after a 100-mV test pulse highlights the kinetic differences in proton accumulation and depletion at the cell surface (Video 1).

To visualize proton depletion using WGA-pHRho, we set up an inward proton gradient and used a potassium pore-blocked (W434F) Shaker-IR mutant (R362H) that creates an omega proton pore upon hyperpolarization (Fig. 2 C, lower right panel). As expected for inward proton flux, the cell surface fluorescence became dimmer upon hyperpolarization, reached steady state, and then recovered with biexponential kinetics when the cell was returned to the 30-mV holding potential (Video 2). All fluorescence changes were due to proton channel expression (Fig. S2 B), as no change in fluorescence was observed when the cells were transiently transfected with empty plasmid DNA (Fig. S2 C).

We next compared WGA-pHRho to WGA-fluorescein (Fig. 2 C). For a fair comparison, we made our own WGA-fluorescein by reacting commercially available FITC with WGA and removed the unreacted fluorophore with a gravity-fed size-exclusion column (Materials and methods). Compared with WGA-pHRho, homemade WGA-fluorescein (Fig. 2 C, green traces) yielded the mirror-opposite response to extracellular proton accumulation (hHv-1) and depletion (Shaker-IR R362H/W434F) with approximately the same current–$\Delta F/F_0$ relationship (Fig. S1 B). As expected, photobleaching was problematic with WGA-fluorescein (the data in Fig. 2 C are uncorrected). The fluorescein photobleaching gives rise to apparent inactivation of the fluorescent signal upon strong depolarizations and obscures the ability to resolve protons diffusing into bulk solution after Hv-1 channel closing (compare WGA-fluorescein to WGA-pHRho in Fig. 2 C). Both fluorescein photobleaching artifacts occur with inward omega proton currents (Fig. 2 C, Shaker-IR R362H/W434F), but the increase in fluorescence partially masks the magnitude of the effect. There was no noticeable difference between commercially available and homemade WGA-fluorescein (Fig. S1 B); thus, for extracellular proton depletion near fluorescein's pKa of 6.4, commercially available WGA-fluorescein was a satisfactory reagent when photobleaching can be reliably corrected.

The exemplars in Fig. 2 C were performed within 1 h of labeling with WGA-pHRho and WGA-fluorescein, which was not technically demanding, but we wondered whether internalization of WGA conjugates would affect the fluorescent signals at the plasma membrane. Up to 1 h after labeling, the majority of the WGA-pHRho appeared to be on the cell surface, as evidenced by the circular labeling (Fig. 2 D); however, bright puncta, indicative of WGA-pHRho internalization, became evident 2 h after labeling and visually overwhelming at 4 h. Surprisingly, the change in fluorescence from hHv-1–expressing cells after a 4-s 80-mV depolarization did not systematically diminish over time (Fig. 2 E), indicating that 4 h after labeling (Fig. 2 D), there were enough pH sensors at the cell surface to detect extracellular proton accumulation and depletion. Part of the surprise was due to the optical illusion created by the overemphasized endocytosed sensors (Fig. 2 D) that were localized in low-pH internal compartments (endosomes and lysosomes). In addition, the data in the latter time points likely favored cells with less internalized WGA-pHRho, because it became noticeably harder over time to make and maintain a gigaohm seal in the whole-cell configuration. Thus, it was possible to visualize proton fluxes from WGA-pHRho–treated cells 4 h after labeling; however, for experimental ease, it was experimentally prudent to image and record immediately after labeling.

To convert the change in fluorescence into pH, we perfused pH standards across cells labeled with WGA-pHRho and WGA-fluorescein and plotted $\Delta F/F_0$ versus pH (Fig. 3 A). Perfusion of pH standards with 1 mM or 10 mM buffer yielded linear responses for both fluorescent WGA-conjugates. Using the linear fits, the fluorescent signals for hHv-1 were converted into ΔpH (Fig. 3 B). The snapshots at 5 s at 0, 20, and 100 mV highlight the advantage of the fluorescence response of WGA-pHRho for detecting extracellular proton accumulation (Fig. 3 C). In addition to seeing proton efflux from the patch-clamped cell (dotted circle), the acidification of the bath solution was revealed by the neighboring WGA-pHRho–labeled cells in Fig. 3 C.

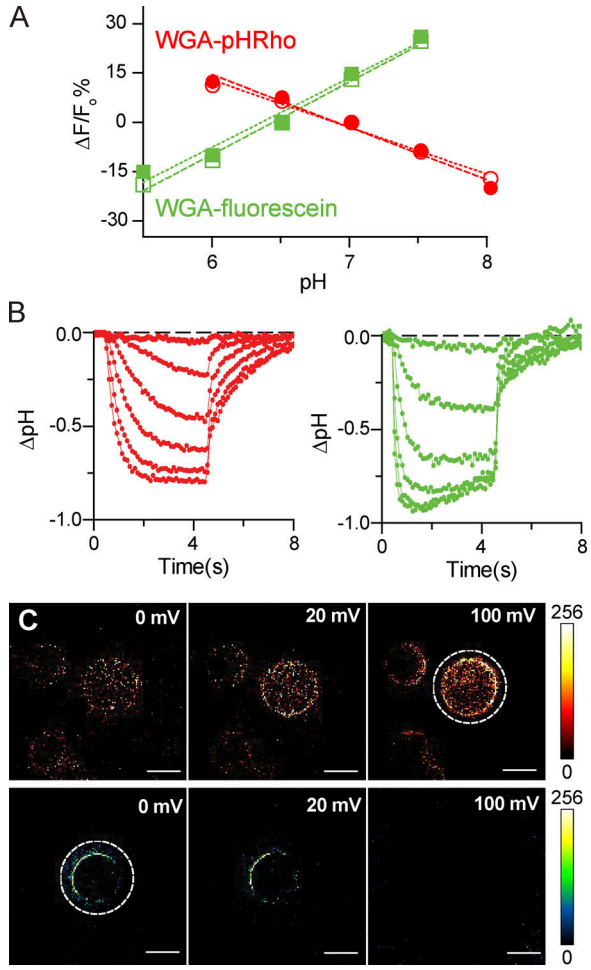

Figure 3. **Cell surface pH calibration of WGA-pHRho and WGA-fluorescein. (A)** CHO cells were labeled with either WGA-fluorescein or WGA-pHRho, and the change of fluorescence ($\Delta F/F_0$%) was plotted using pH standards (HEPES; 1 mM, open symbols; 10 mM, closed symbols); F_o was chosen to be at the approximate pKa of each sensor (pH 7.0 for WGA-pHRho and pH 6.5 for WGA-fluorescein). The linear fits for WGA-pHRho were pH = 6.99 − 0.06 × [$\Delta F/F_0$] and pH = 6.91 − 0.07 × [$\Delta F/F_0$] for 1 and 10 mM, respectively; the linear fits for WGA-fluorescein were pH = 6.51 + 0.05 × [$\Delta F/F0$] and pH = 6.52 + 0.05 × [$\Delta F/F_0$] for 1 and 10 mM, respectively. **(B)** Conversion of $\Delta F/F_0$ (%) to CHO cells expressing hHv-1 were held at −80 mV, and changes in fluorescence were elicited from 4-s depolarizations from 0 to 100 mV in 20-mV increments and converted into ΔpH using the calibration curves in A; WGA-pHRho, red; WGA-fluorescein, green. **(C)** $\Delta F/F_0$ images of cells expressing hHv-1 taken at 4 s shown in B. Top: WGA-pHRho; bottom: WGA-fluorescein. Dotted white circles indicate the voltage-clamped cell. White scale bars represent 10 µm.

Because fluorescent WGA conjugates are routinely used to demarcate the plasma membrane of isolated cardiomyocytes (Stegemann et al., 1990), we next determined whether WGA-pHRho could differentially detect lactate-coupled proton transport in the t-tubules and at the sarcolemma (Fig. 4). To spatiotemporally detect t-tubular and sarcolemma proton fluxes, we used structured light microscopy (Materials and methods) to rapidly illuminate a single *z*-plane (~700 nm thick) 2 µm into the cardiomyocyte. Fig. 4 A shows an illuminated *z*-plane from a WGA-pHRho–labeled rat ventricular myocyte. Perfusion of 10 mM lactate (Fig. 4 B) resulted in a rapid loss of fluorescence that quickly reversed and then slowly approached steady state, indicative of lactic acid entering the cell. Washout of extracellular lactate led to a rapid efflux of protons from the cell that diminished slowly over time. Lactate-induced proton transport was inhibited with the MCT inhibitor AR-C155858 (50 nM), suggesting that cardiac MCT-1 was responsible for lactic acid transport into the cell. In contrast, proton efflux after lactate washout was likely an amalgam of both cardiac MCT-1 and Nhe1 (Na^+/H^+) activity (Jóhannsson et al., 1997; Petrecca et al., 1999). To isolate the sarcolemma and t-tubule signals, we analyzed concentric annuli by systematically eroding five pixels from the cardiomyocyte edge (Fig. 4 C). Annulus 0 (A0) contained primarily signal from the sarcolemma, whereas the signal from the next three annuli (A1–A3) were increasingly enriched with t-tubules (Fig. 4 D). Because the mean of WGA-pHRho labeling varied <1% between annuli (Fig. 4 E), the absolute change of fluorescence corresponds to the ion concentration for each annulus and was compared (Fig. 4 F). Starting at the sarcolemma (A0), the initial change in fluorescence upon lactate perfusion increased significantly ($P < 0.05$) when compared with the inner annulus until A2, where there was no significant difference between the A2 and A3 annuli. In contrast, the initial change in fluorescence upon lactate washout was not significant when comparing adjacent annuli, but significant differences in initial fluorescence were measured between nonneighboring annuli. Taken together, these results demonstrate that the initial MCT-1 activity results in significantly more proton depletion in the t-tubules compared with the sarcolemma.

We next determined whether WGA-pHRho could detect proton efflux from primary neuron–astrocyte cocultures. Cocultures (6–10 d) obtained from mice cortex were labeled with WGA-pHRho in free glucose media, rinsed with free glucose media, and imaged by means of laser scanning microscopy. When cocultured, neurons and astrocytes organize such that astrocytes occupy the bottom of the chamber, while most of the neurons grow on top (Vicario-Abejón, 2004; Aras et al., 2008). Therefore, two optical planes were imaged to capture both cell types that were identified by their distinctive morphologies. Fig. 5 A is a representative merged image of the neuronal and astrocyte planes labeled with WGA-pHRho and DAPI. To elicit lactic acid efflux, glucose-starved cocultures were exposed to glucose (3 mM) while following the WGA-pHRho signal during acquisition. Merged neuronal and astrocyte planes (Fig. 5, B and C) show the average change in fluorescence induced by the addition of glucose to the media (Fig. 5 D). As expected, an increase in the substrate of the glycolytic chain was accompanied with an increase in the release of protons (Fig. 5, E and F), an indirect readout for lactic acid release, presumably through MCTs (Dimmer et al., 2000). The overall effect of glucose addition was similar in both cell types (Fig. 5 G); however, poisoning the mitochondrial respiratory chain with rotenone (100 µM; Fig. 5 D) led to clear differences in their response. Although lactic acid efflux from astrocytes (Fig. 5 F) was relatively unaffected by rotenone in the Fig. 5 B exemplar, an increase of lactic acid efflux from neurons was observed (Figs. 5, E and G). There was no correlation between the glucose response (or the lack

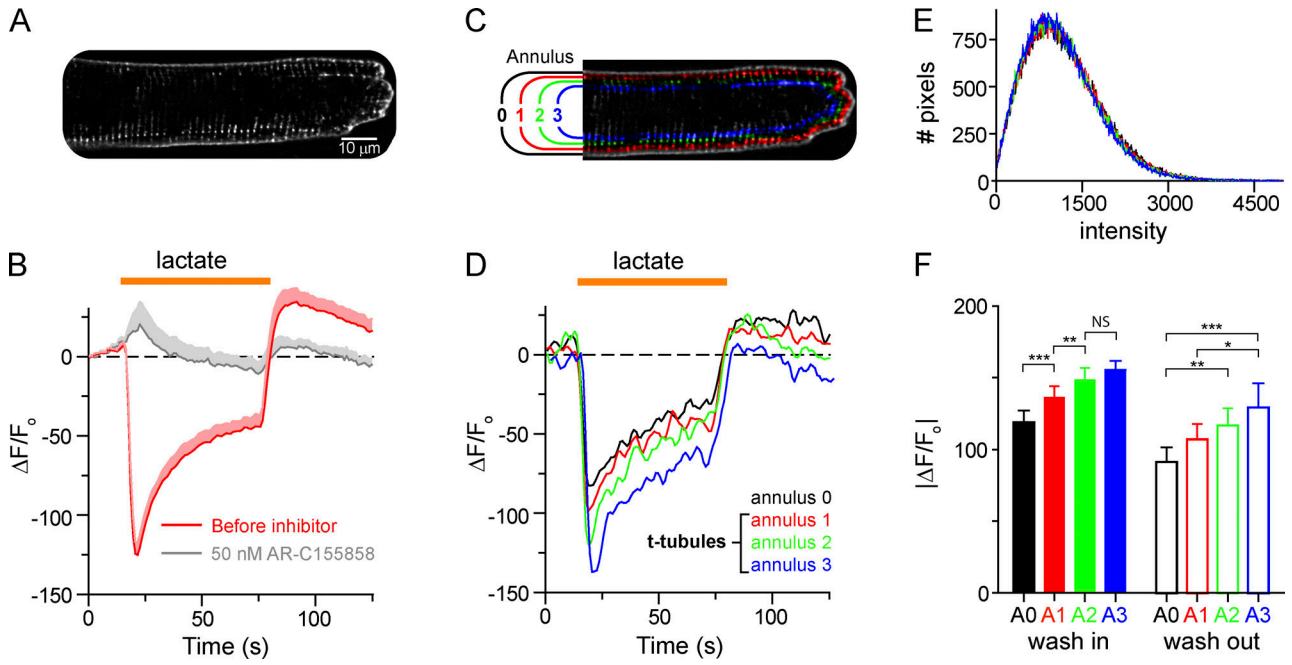

Figure 4. **Structured light microscopy of lactate-stimulated proton transport in rat ventricular myocytes labeled with WGA-pHRho. (A)** A ∼750-nm illuminated *z*-plane of a WGA-pHRho–labeled ventricular myocyte ∼2 µm above the coverslip focal plane. **(B)** Time course of 10 mM lactate perfusion before (red) and after addition of 50 nM AR-C155858 (gray). Plotted data are mean + SEM (shading) for clarity (n = 6 cells); data were collected at 1 Hz. **(C)** Pseudocolor image depicting the eroding pixel (5 px) analysis to generate the four annuli. **(D)** Changes of $\Delta F/F_0$ before, during, and after perfusion of 10 mM lactate at each annulus (A0–A3). **(E)** Pixel intensity histogram of the four annuli (area normalized) for cell shown in A. **(F)** Average maximal $|\Delta F/F_0|$ upon wash in (solid bars) and wash out (open bars) of 10 mM lactate for nine cells. One-way ANOVA (Bonferroni's multiple comparison test) was used to determine significance (*, P < 0.05; **, P < 0.01; ***, P < 0.001). Error bars represent SEM.

thereof) and the subsequent rotenone response in cocultures from three animals (Fig. 5 H). Fig. 5 I shows glucose and rotenone responses from five plates of cocultures (19 neurons and 21 astrocytes in total). These results are consistent with previous reports (Magistretti and Allaman, 2015) that mitochondrial oxidative capacity is greater in neurons than astrocytes in coculture.

Discussion

We sought to circumvent the secretory pathway and exploit WGA binding to mammalian glycocalyces to develop a simple, nongenetic approach to fluorescently visualize extracellular proton accumulation and depletion from isolated cells. Despite binding to sialic acid and N-acetylglucosamine (Monsigny et al., 1980), the voltage gating of glycosylated and nonglycosylated ion channels was not substantially altered after WGA treatment (Fig. 2 B). Because WGA labeling over the entire cell surface was uniform, with only a 1% difference in labeling intensity (Fig. 4 E) between annuli, the change in fluorescence ($\Delta F/F_0$) can be reliably converted into a change in pH (Fig. 3). Because the buffer capacity must be kept very low to observe changes in pH with either WGA conjugate, using this approach to measure a precise pH value adjacent to the extracellular surface in an extremely low buffered solution is not recommended. The pros of the rhodamine-based WGA-pHRho are that it is photostable, it increases its fluorescence upon protonation, and it has a pKA ∼7 (Aigner et al., 2012) that is well matched for extracellular pH determinations. If photobleaching can be corrected, then WGA-fluorescein is better than WGA-pHRho for visualizing proton influx, because it is commercially available and becomes brighter upon alkalization.

Labeling with WGA conjugates has several advantages over our previously published small-molecule approach (Zhang et al., 2016). First, it does not require the cells to metabolize the unnatural sugar, enabling facile labeling of primary cardiomyocytes and neuron–astrocyte cocultures. Second, very little intracellular labeling was initially observed, because WGA conjugates are not membrane permeant. However, because WGA-pHRho targets cell surface glycoproteins, the fluorescent pH sensors are internalized over time, leading to unaesthetic bright puncta, because WGA-pHRho is more fluorescent in acidic compartments. Although changes in fluorescence can be observed >3 h after labeling (Fig. 2 E), rapid cell surface labeling and subsequent imaging is a major advantage of using WGA conjugates to detect extracellular proton accumulation and depletion over the landscape of a cell.

To demonstrate the utility of WGA conjugates for detecting spatiotemporal differences in extracellular proton accumulation and depletion, we labeled primary ventricular cardiomyocytes and neuron–astrocyte cocultures with WGA-pHRho and imaged at several *z*-planes. Using structured illumination at single *z*-plane, we observed significantly more lactic acid depletion in annuli enriched with t-tubules. Although the initial influx of lactic acid can be attributed to MCT-1, the larger pH change observed in the t-tubules could be due to either more

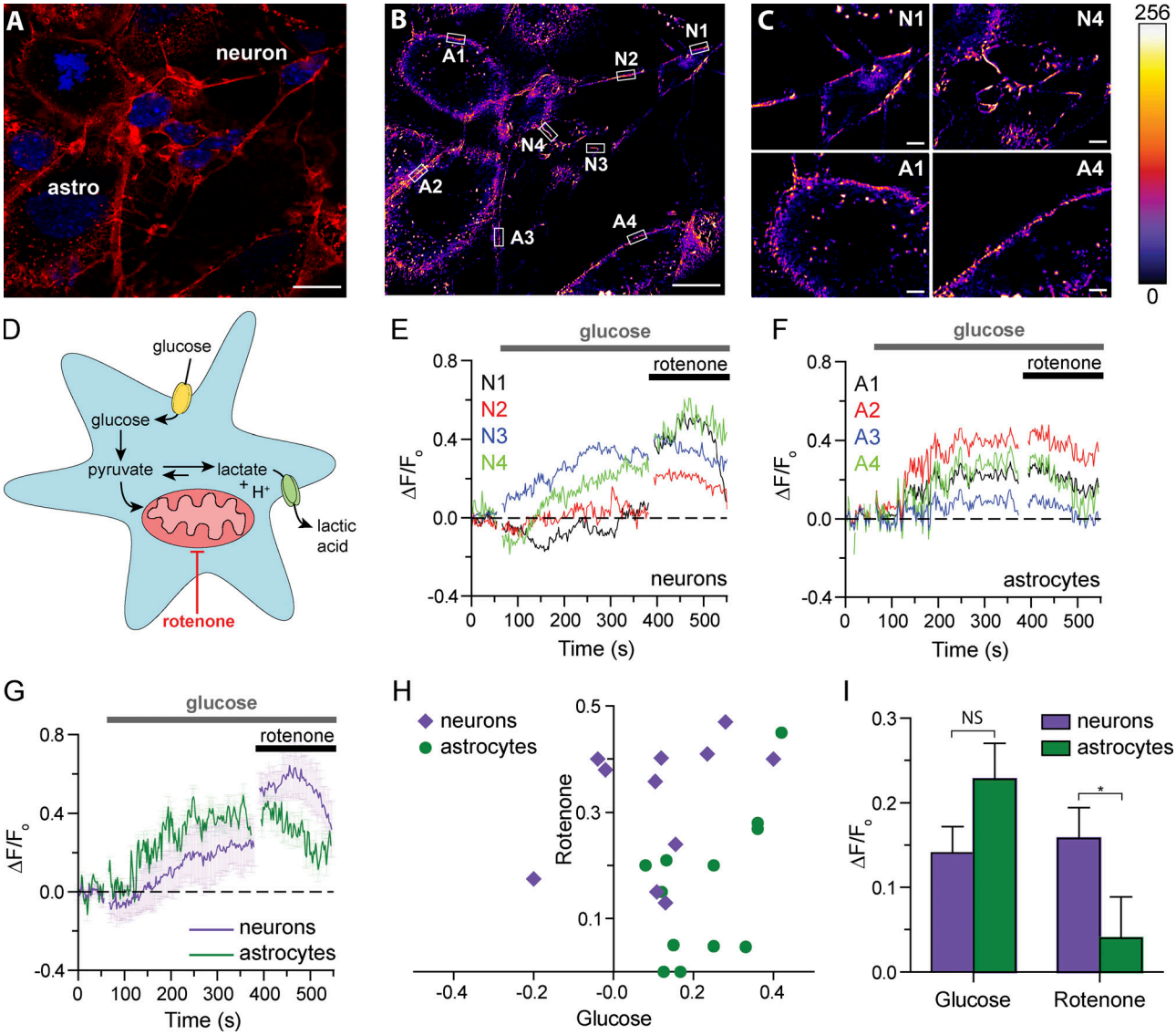

Figure 5. **Proton efflux from primary neuron–astrocyte cocultures labeled with WGA-pHRho. (A)** Merged Airyscan image of the neuronal and astrocyte planes labeled with WGA-pHRho (red) and DAPI (blue). **(B)** Pseudocolor image showing the averaged $\Delta F/F_0$ of the regions of interest (ROI) in A after glucose addition. Red shades indicate more activity over time. ROI are denoted by white boxes (A, astrocyte; N, neuron). Data were collected at 2 Hz. Scale bars represent 10 µm in A and B. **(C)** Magnified images of two astrocytes and neurons in B to show labeling coverage; 8-bit pseudo-color intensity scale bar is for panels in B and C. Scale bars represent 2 µm. **(D)** Cartoon depiction of the metabolic pathways expected to be affected by glucose starvation and rotenone mitochondrial poisoning. **(E and F)** Time courses of the (E) neuronal and (F) astrocytic pHRho signal during glucose (3 mM) and rotenone (100 µM) addition for the exemplar in B. **(G)** Averaged data from E and F (total number of cells in the plot: four neurons and four astrocytes from one single dish; this average is considered $n = 1$). Error bars represent SEM. **(H)** Variation of the neuronal and astrocytic responses to glucose and rotenone; 11–12 ROIs from dishes from three animals. **(I)** Maximal change in $\Delta F/F_0$ ($n = 4$–6 dishes) for glucose and rotenone treatment, comprising a total of 19 neurons and 21 astrocytes in total; error bars represent SEM. A paired *t* test was used to determine significance (*, $P < 0.05$).

MCT-1 transporters localized to the t-tubules and/or the restricted exchange with bulk solution due to the architecture and membrane folds of the t-tubule network. The pixel intensity histogram (Fig. 4 E) shows uniform labeling of the annuli with WGA-pHRho; however, it is unclear whether WGA-pHRho labels the narrower nooks and crannies of the cardiac tubular network. A lipid-conjugated pHRho or trapping a small-molecule, membrane-impermeant, fluorescent pH sensor in the extracellular t-tubule network (Launikonis et al., 2018) may be better suited to investigate the narrowest cardiac t-tubules as well as the skeletal t-tubular system. For neuron–astrocyte cocultures, WGA-pHRho and imaging on two alternating planes revealed differences between neuronal and astrocytic proton fluxes and mitochondrial oxidative capacity. In both experimental paradigms, we used WGA-pHRho to detect the proton that is co-transported with lactate, which is prone to contamination by other proton-coupled (and bicarbonate) transporters in primary cells that are attempting to regulate intracellular pH. WGA conjugates with small-molecule (Pal et al., 2009) or protein-based (San Martín et al., 2013) fluorescent lactate sensors would allow

more specific detection of extracellular lactic acid accumulation and depletion in a well-buffered external solution.

In summary, WGA-pHRho is easy to make, and it quickly and specifically labels the glycocalyx of primary cells in culture. WGA-pHRho is ideal for detecting proton accumulation, and its photostability makes it compatible for use with several imaging modalities. As a nongenetically encoded approach, it is amenable for usage with human cells and humans as WGA-fluorescein has been used to visualize the ocular glycocalyx of soft contact lens wearers (Fukui et al., 2016). The straightforward labeling and purification procedures outlined herein will allow for the synthesis of WGA pH-sensitive conjugates with various pKa values and excitation and emission maxima. Moreover, the approach is readily generalizable to other small-molecule ion-sensitive fluorophores that possess pendant carboxylic handles that can be conjugated to WGA.

Acknowledgments

Merritt C. Maduke served as editor.

This work was supported by the National Institutes of Health (grant GM-070650 to W.R. Kobertz) and the US/Chile Fulbright Scholar Program (W.R. Kobertz).

The authors declare no competing financial interests.

Author contributions: L. Zhang synthesized pHRho and developed the WGA derivatization procedure. M. Zhang performed the CHO and cardiomyocyte experiments. The patch-clamp fluorometry setup was built by K. Bellve; structured illumination data were acquired on TESM, analyzed by K. Fogarty, and were built and are maintained by K. Fogarty and K. Bellve. M.A. Castro designed the glucose/rotenone experiments and prepared the astrocyte–neuron cocultures. S. Brauchi labeled, imaged, and analyzed the coculture data. W.R. Kobertz designed the experiments, created the figures, and wrote the manuscript. All authors approved the final version of the manuscript.

Submitted: 24 September 2019
Accepted: 3 January 2020

References

Aigner, D., S.M. Borisov, F.J. Fernández, J.F. Fernández Sánchez, R. Saf, and I. Klimant. 2012. New fluorescent pH sensors based on covalently linkable PET rhodamines. *Talanta.* 99:194–201. https://doi.org/10.1016/j.talanta.2012.05.039

Aras, M.A., K.A. Hartnett, and E. Aizenman. 2008. Assessment of cell viability in primary neuronal cultures. *Curr. Protoc. Neurosci.* Chapter 7: Unit 7.18.

Colecraft, H.M., B. Alseikhan, S.X. Takahashi, D. Chaudhuri, S. Mittman, V. Yegnasubramanian, R.S. Alvania, D.C. Johns, E. Marbán, and D.T. Yue. 2002. Novel functional properties of Ca(2+) channel beta subunits revealed by their expression in adult rat heart cells. *J. Physiol.* 541: 435–452. https://doi.org/10.1113/jphysiol.2002.018515

Dimmer, K.-S., B. Friedrich, F. Lang, J.W. Deitmer, and S. Bröer. 2000. The low-affinity monocarboxylate transporter MCT4 is adapted to the export of lactate in highly glycolytic cells. *Biochem. J.* 350:219–227. https://doi.org/10.1042/bj3500219

Fukui, M., M. Yamada, Y. Akune, C. Shigeyasu, and K. Tsubota. 2016. Fluorophotometric Analysis of the Ocular Surface Glycocalyx in Soft Contact Lens Wearers. *Curr. Eye Res.* 41:9–14. https://doi.org/10.3109/02713683.2014.999948

Jóhannsson, E., E.A. Nagelhus, K.J. McCullagh, O.M. Sejersted, T.W. Blackstad, A. Bonen, and O.P. Ottersen. 1997. Cellular and subcellular expression of the monocarboxylate transporter MCT1 in rat heart. A high-resolution immunogold analysis. *Circ. Res.* 80:400–407. https://doi.org/10.1161/01.res.0000435856.47954.71

Johnson, D., and E.S. Bennett. 2008. Gating of the shaker potassium channel is modulated differentially by N-glycosylation and sialic acids. *Pflugers Arch.* 456:393–405. https://doi.org/10.1007/s00424-007-0378-0

Johnson, D., M.L. Montpetit, P.J. Stocker, and E.S. Bennett. 2004. The sialic acid component of the beta1 subunit modulates voltage-gated sodium channel function. *J. Biol. Chem.* 279:44303–44310. https://doi.org/10.1074/jbc.M408900200

Launikonis, B.S., T.R. Cully, L. Csernoch, and D.G. Stephenson. 2018. NHE- and diffusion-dependent proton fluxes across the tubular system membranes of fast-twitch muscle fibers of the rat. *J. Gen. Physiol.* 150: 95–110. https://doi.org/10.1085/jgp.201711891

Lobas, M.A., R. Tao, J. Nagai, M.T. Kronschläger, P.M. Borden, J.S. Marvin, L.L. Looger, and B.S. Khakh. 2019. A genetically encoded single-wavelength sensor for imaging cytosolic and cell surface ATP. *Nat. Commun.* 10:711. https://doi.org/10.1038/s41467-019-08441-5

Magistretti, P.J., and I. Allaman. 2015. A cellular perspective on brain energy metabolism and functional imaging. *Neuron.* 86:883–901. https://doi.org/10.1016/j.neuron.2015.03.035

Marvin, J.S., B.G. Borghuis, L. Tian, J. Cichon, M.T. Harnett, J. Akerboom, A. Gordus, S.L. Renninger, T.W. Chen, C.I. Bargmann, et al. 2013. An optimized fluorescent probe for visualizing glutamate neurotransmission. *Nat. Methods.* 10:162–170. https://doi.org/10.1038/nmeth.2333

Monsigny, M., A.-C. Roche, C. Sene, R. Maget-Dana, and F. Delmotte. 1980. Sugar-lectin interactions: how does wheat-germ agglutinin bind sialoglycoconjugates? *Eur. J. Biochem.* 104:147–153. https://doi.org/10.1111/j.1432-1033.1980.tb04410.x

Navaroli, D.M., K.D. Bellvé, C. Standley, L.M. Lifshitz, J. Cardia, D. Lambright, D. Leonard, K.E. Fogarty, and S. Corvera. 2012. Rabenosyn-5 defines the fate of the transferrin receptor following clathrin-mediated endocytosis. *Proc. Natl. Acad. Sci. USA.* 109:E471–E480. https://doi.org/10.1073/pnas.1115495109

Neil, M.A.A., R. Juškaitis, and T. Wilson. 1997. Method of obtaining optical sectioning by using structured light in a conventional microscope. *Opt. Lett.* 22:1905–1907.

Noma, K., K. Kimura, K. Minatohara, H. Nakashima, Y. Nagao, A. Mizoguchi, and Y. Fujiyoshi. 2009. Triple N-glycosylation in the long S5-P loop regulates the activation and trafficking of the Kv12.2 potassium channel. *J. Biol. Chem.* 284:33139–33150. https://doi.org/10.1074/jbc.M109.021519

Pal, R., D. Parker, and L.C. Costello. 2009. A europium luminescence assay of lactate and citrate in biological fluids. *Org. Biomol. Chem.* 7:1525–1528. https://doi.org/10.1039/b901251f

Patriarchi, T., J.R. Cho, K. Merten, M.W. Howe, A. Marley, W.-H. Xiong, R.W. Folk, G.J. Broussard, R. Liang, M.J. Jang, et al. 2018. Ultrafast neuronal imaging of dopamine dynamics with designed genetically encoded sensors. *Science.* 360:eaat4422. https://doi.org/10.1126/science.aat4422

Pendin, D., E. Greotti, K. Lefkimmiatis, and T. Pozzan. 2017. Exploring cells with targeted biosensors. *J. Gen. Physiol.* 149:1–36. https://doi.org/10.1085/jgp.201611654

Petrecca, K., R. Atanasiu, S. Grinstein, J. Orlowski, and A. Shrier. 1999. Subcellular localization of the Na+/H+ exchanger NHE1 in rat myocardium. *Am. J. Physiol.* 276:H709–H717. https://doi.org/10.1152/ajpheart.1999.276.2.H709

San Martín, A., S. Ceballo, I. Ruminot, R. Lerchundi, W.B. Frommer, and L.F. Barros. 2013. A genetically encoded FRET lactate sensor and its use to detect the Warburg effect in single cancer cells. *PLoS One.* 8:e57712. https://doi.org/10.1371/journal.pone.0057712

Schroeder, M.A., M.A. Ali, A. Hulikova, C.T. Supuran, K. Clarke, R.D. Vaughan-Jones, D.J. Tyler, and P. Swietach. 2013. Extramitochondrial domain rich in carbonic anhydrase activity improves myocardial energetics. *Proc. Natl. Acad. Sci. USA.* 110:E958–E967. https://doi.org/10.1073/pnas.1213471110

Schwetz, T.A., S.A. Norring, A.R. Ednie, and E.S. Bennett. 2011. Sialic acids attached to O-glycans modulate voltage-gated potassium channel gating. *J. Biol. Chem.* 286:4123–4132. https://doi.org/10.1074/jbc.M110.171322

Stegemann, M., R. Meyer, H.G. Haas, and M. Robert-Nicoud. 1990. The cell surface of isolated cardiac myocytes--a light microscope study with use of fluorochrome-coupled lectins. *J. Mol. Cell. Cardiol.* 22:787–803. https://doi.org/10.1016/0022-2828(90)90090-O

Stock, C., M. Mueller, H. Kraehling, S. Mally, J. Noël, C. Eder, and A. Schwab. 2007. pH nanoenvironment at the surface of single melanoma cells. *Cell. Physiol. Biochem.* 20:679–686. https://doi.org/10.1159/000107550

Sun, F., J. Zeng, M. Jing, J. Zhou, J. Feng, S.F. Owen, Y. Luo, F. Li, H. Wang, T. Yamaguchi, et al. 2018. A Genetically Encoded Fluorescent Sensor Enables Rapid and Specific Detection of Dopamine in Flies, Fish, and Mice. *Cell.* 174:481–496.e19. https://doi.org/10.1016/j.cell.2018.06.042

Vicario-Abejón, C. 2004. Long-term culture of hippocampal neurons. *Curr. Protoc. Neurosci.* Chapter 3:Unit 3.2.

Villafuerte, F.C., P. Swietach, J.-B. Youm, K. Ford, R. Cardenas, C.T. Supuran, P.M. Cobden, M. Rohling, and R.D. Vaughan-Jones. 2014. Facilitation by intracellular carbonic anhydrase of Na+ -HCO3- cotransport but not Na+/H+ exchange activity in the mammalian ventricular myocyte. *J. Physiol.* 592:991–1007. https://doi.org/10.1113/jphysiol.2013.265439

Zhang, L., K. Bellve, K. Fogarty, and W.R. Kobertz. 2016. Fluorescent Visualization of Cellular Proton Fluxes. *Cell Chem. Biol.* 23:1449–1457. https://doi.org/10.1016/j.chembiol.2016.10.013

Supplemental material

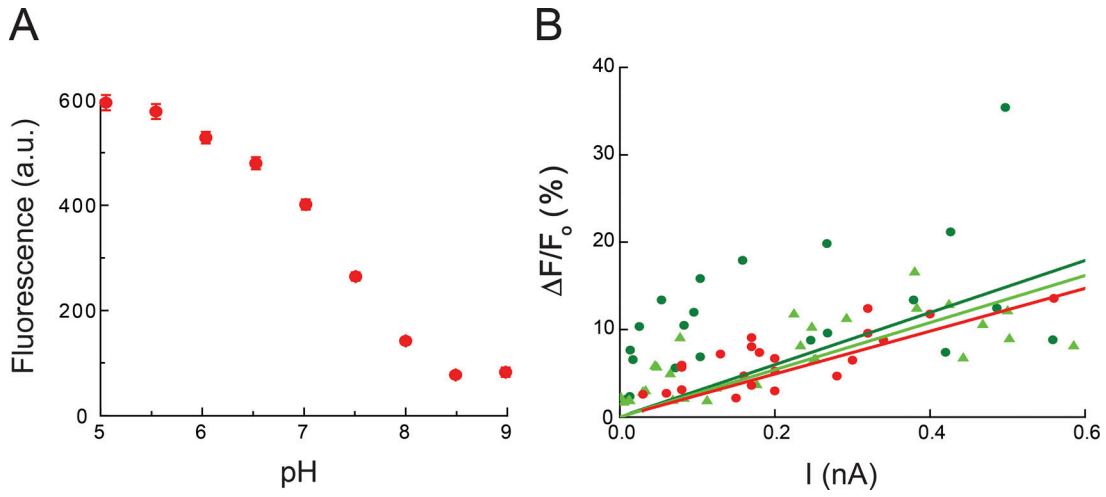

Figure S1. **Characterization of pH-sensitive WGA conjugates, related to Fig. 2. (A)** Fluorescence-pH plot of WGA-pHRho in solution; excitation wavelength, 550 nm. a.u., arbitrary units. **(B)** $\Delta F/F_0$-I plot of WGA-pHRho (red), homemade WGA-fluorescein (dark green), and WGA-fluorescein from Vector Laboratories (light green).

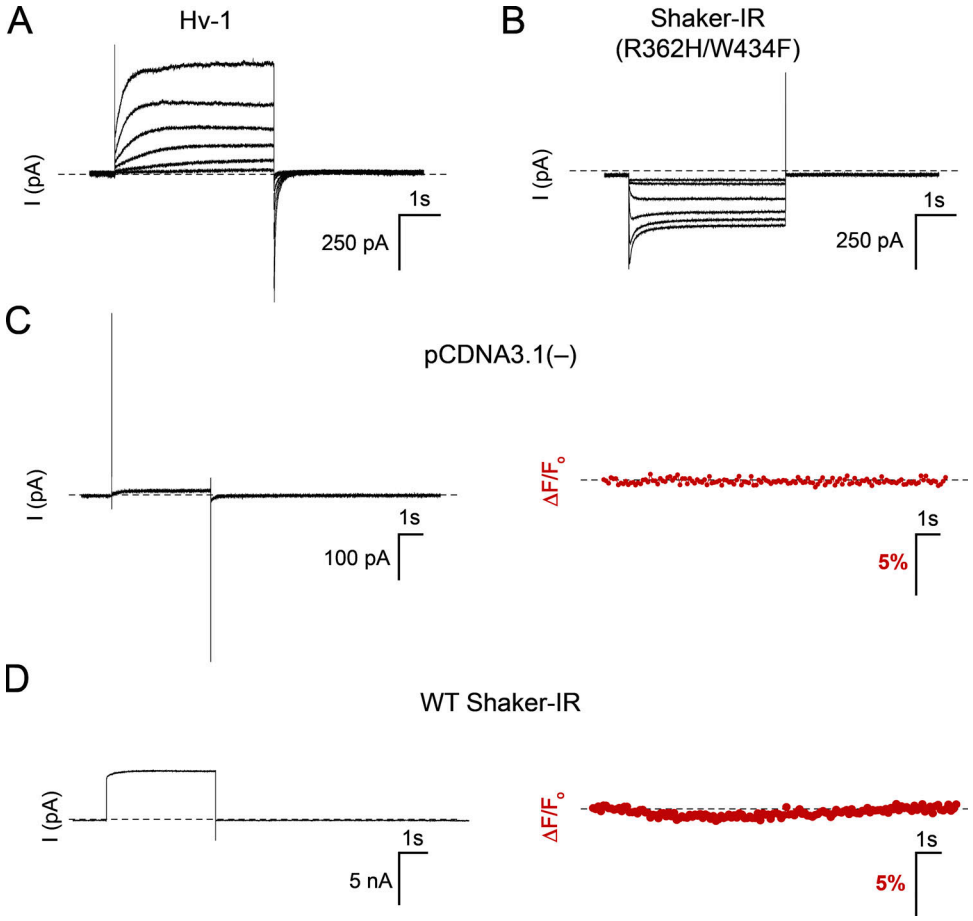

Figure S2. **Changes in WGA-pHRho fluorescence requires exogenous expression of proton channels in CHO cells. Related to Fig. 2. (A and B)** Current–voltage relationships for (A) Hv-1 and (B) Shaker-IR (R362H/W434F) expressed in CHO cells. Hv-1 was held at −80 mV, and currents were elicited from 4-s command voltages from 0 to 100 mV in 20-mV increments; Shaker-IR (R362H/W434F) was held at 30 mV, and the currents were elicited from 4-s command voltages from −120 to −20 mV in 20-mV increments. **(C and D)** Voltage-clamp fluorometry of CHO cells transfected with either (C) pCDNA3.1(–) or (D) WT Shaker-IR controls. The cells were held at −80 mV and depolarized to for 4 s; pCDNA3.1(–), 100 mV; WT Shaker-IR, 20 mV. An outward pH gradient (pH_o/pH_i = 7.5/6.0) was used in A and C, and an inward pH gradient (pH_o/pH_i = 6.0/7.5) was used in B and D. The buffer (HEPES) capacity was 0.1 mM for all experiments.

Video 1. **$\Delta F/F_0$ movie of a representative CHO cell expressing Hv-1, related to Figs. 2 C and 3 C.** The cell was held at −80 mV and depolarized at 100 mV for 4 s. F_0 is the fluorescent signal of the first frame; the frame rate is 10 frames per second. The patch-clamped cell becomes the brightest cell in the center of the frame upon depolarization. Under the low–buffer capacity conditions (0.1 mM HEPES), the fluorescence of the WGA-pHRho–labeled neighboring cells record the proton wavefront emanating and dissipating from the patch-clamped cell.

Video 2. **Raw fluorescent images of a representative CHO cell expressing Shaker-IR (R362H/W434F) labeled with WGA-pHRho, related to Figs. 2 C and 3 C.** The cell was held at 30 mV and hyperpolarized to −120 mV for 4 s. The patch-clamped cell is denoted with an arrow; the frame rate is 10 frames per second.